We are IntechOpen,
the world's leading publisher of
Open Access books
Built by scientists, for scientists

6,900
Open access books available

185,000
International authors and editors

200M
Downloads

154
Countries delivered to

Our authors are among the

TOP 1%
most cited scientists

12.2%
Contributors from top 500 universities

CLARIVATE ANALYTICS
BOOK CITATION INDEX
INDEXED

WEB OF SCIENCE™

Selection of our books indexed in the Book Citation Index
in Web of Science™ Core Collection (BKCI)

Interested in publishing with us?
Contact book.department@intechopen.com

Numbers displayed above are based on latest data collected.
For more information visit www.intechopen.com

5

Ultrasonic Waves on Gas Hydrates Experiments

Gaowei Hu and Yuguang Ye
Qingdao Institute of Marine Geology
China

1. Introduction

In this chapter, the acoustic properties of gas hydrate-bearing sediments are investigated experimentally. The flat-plate transducers and a new kind of bender elements are developed to measure both compressional wave velocity (Vp) and shear wave velocity (Vs) of hydrated consolidated sediments and hydrated unconsolidated sediments, respectively. The main purpose is to construct a relation between gas hydrate saturation and acoustic velocities of the hydrate-bearing sediments, with which we can give suggestions on the usage of various velocity-models in field gas hydrate explorations.

Gas hydrates, or clathrates, are ice-like crystalline solids composed of water molecules surrounding gas molecules (usually methane) under certain pressure and temperature conditions [Sloan, 1998]. In recent years, gas hydrates have been widely studied because of their potential as a future energy resource [Kvenvolden, 1998; Milkov and Sassen, 2003], their important role in the global carbon cycle and global warming [Dickens, 2003; Dickens, 2004], and their potential as a geotechnical hazard [Brown et al., 2006; Pecher et al., 2008]. To assess the impact of gas hydrates within these areas of interest, an understanding of their distribution within the seabed and their relationship with the host sediment is essential and helpful.

Seismic techniques have been widely used for mapping and quantifying gas hydrates in oceanic sediments [Shipley et al., 1979; Holbrook et al., 1996; Carcione and Gei, 2004]. In general, gas hydrates exhibit relatively high elastic velocities (both Vp and Vs), compared to the pore-filling fluids; therefore, the velocity of gas hydrate-bearing sediments is usually elevated [Stoll, 1974; Tucholke et al., 1977]. To quantify the amount of gas hydrate or to infer the physical properties of gas hydrate-bearing sediments, an understanding of the relationship between the amount of gas hydrate in the pore space of sediments and the elastic velocities is needed.

Two different approaches were used to relate the hydrate saturation and velocity in oceanic sediments: (1) empirical methods including Wyllie's time average [Wyllie et al., 1958; Pearson et al., 1983], Wood's equation [Wood, 1941] and weighted combinations of the Wyllie's time average and Wood's equation [Lee et al., 1996], and (2) physics-based models, such as the effective medium theory (EMT) [Helgerud et al., 1999; Dvorkin and Prasad, 1999] and the Biot-Gassmann theory modified by Lee (BGTL) [Lee, 2002a, 2002b, 2003]. However, the gas hydrate volumes within sediments estimated with these approaches are quite different. Chand et al. [2004] made a comparison of four current models, i.e., the WE (Weighted Equation) [Lee et al., 1996], the EMT, the three-phase Biot theory (TPB) [Carcione

and Tinivella, 2000; Gei and Carcione, 2003] and the differential effective medium theory (DEM) [Jakobsen et al., 2000], in predicting hydrate saturation with field data sets obtained from ODP Leg 164 on Blake Ridge, and from the Mallik 2L-38 well, Mackenzie Delta, Canada. The results show that three of the models predict consistent hydrate saturation of 60-80% for the Mallik 2L-38 well, but the EMT model predicts 20 per cent higher. For the clay-rich sediments of Blake Ridge, the DEM, EMT and WE models predict 10-20% hydrate saturation, which is similar to the result inferred from resistivity data, but lower than the result predicted by the TPB model. Ojha and Sain [2008] estimated the saturation of gas hydrate at Makran accretionary prism using the BGTL and EMT models. The BGTL model shows hydrate saturation of 7-9%, but the EMT model predicts the saturation of gas hydrate as 14-33%. Apparently, it is important to validate these elastic velocity models with data obtained from synthesized hydrate-bearing sediment in the laboratory.

The relationship between acoustic velocities and hydrate saturation has been studied in laboratory by several researchers. Although the experimental results may not automatically be applied to the seismic frequencies of field data, however, as the general variability of acoustic velocities with the variable pore fluid is similar with that of seismic velocities [Sothcott et al., 2000], the experiments can provide some basic geophysical parameters for the exploration of gas hydrate reservoirs.

2. Ultrasonic waves in hydrate-bearing consolidated sediments

In this section, acoustic properties of gas hydrate-bearing consolidated sediments are investigated experimentally. Gas hydrate was formed and subsequently dissociated in consolidated sediments. In the whole process, ultrasonic methods and Time Domain Reflectometry (TDR) are simultaneously used to measure the acoustic properties and hydrate saturations of the host sediments, respectively. The whole experimental processes and results are presented here.

2.1 Methods

It's needed to keep a suitable circumstance, e.g. a certain high pressure and low temperature, for measuring parameters of hydrate-bearing sediments. Thus, ultrasonic method and TDR technique used in this study are a little different from their conventional ways because they must sustain pressure during the measurements. A characteristic of our methods is that real-time measurements of both hydrate saturation and acoustic velocities were conducted in one system.

2.1.1 Ultrasonic method

P wave and S wave velocities were measured by transmission using two transducers (0.5 MHz frequency) placed at each end of the cylindrical core (Fig. 1). Signals were digitized by a CompuScope card from GaGe Applied Technologies. Because the CompuScope 14100 is a 14 bit, 50 million samples per second dual-channel waveform digitizer card and data transfer rates from the Compu-Scope memory to PC memory run as high as 80 Mb s^{-1}, it is thought that the CompuScope card caused few errors in velocity estimation. However, the errors in velocity estimation resulted mainly from picking t_1 and t_2, which are the travel times of the compressional and shear waves, respectively (Fig. 2). The velocities were calculated by Vp =

$L/(t_1 - t_0)$ and $V_s = L/(t_2 - t_0)$, where L is the sample length and t_0 is the inherent travel time of the transducers. Two different lengths of standardized cylindrical aluminum rods were used to calibrate the t_0 of the transducers. The final errors in estimating compressional wave velocity and shear wave velocity were ±1.2% (±50 m s^{-1}) and ±1.6% (±40 m s^{-1}), respectively. The amplitudes of compressional and shear waves can be read directly (Fig. 2).
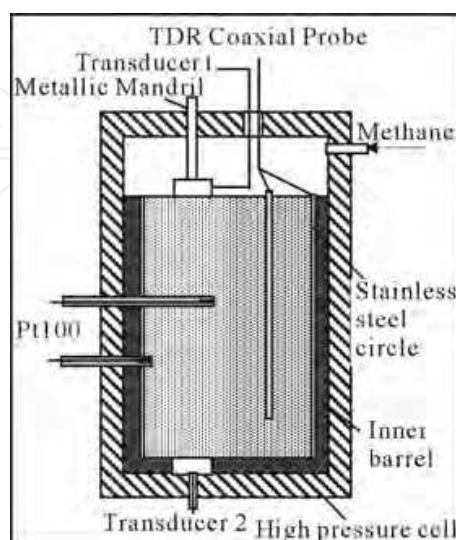

Fig. 1. Cross section through the high-pressure vessel. A single probe and a stainless steel circle around the cylindrical core are two poles of the TDR coaxial probe.
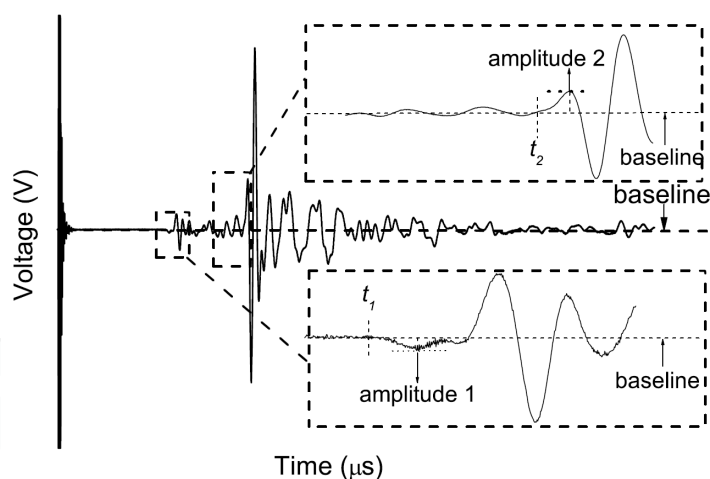
Fig. 2. Ultrasonic waveform measured by flat-plate tranducers. Arrival times of the first arrival wave of compressional and shear waves are t_1 and t_2, respectively. Amplitude 1 and amplitude 2 represent the amplitudes of compressional and shear waves, respectively.

2.1.2 TDR technique

TDR was initially used for detecting the position of breaks in transmission line cables. The technique was introduced to measure water contents of soil samples in 1980s, and then it developed rapidly [Topp et al., 1980; Dalton et al., 1986]. Topp et al. [1980] was probably the first one who measured water contents of soil samples with TDR technique. They found a practical relation between dielectric constants and water contents of the soil samples based

on various types of experimental results. With regard to some particular substance, special calibration is needed before measurements. For example, Regalado et al. [2003] proposed a empirical equation for calculating water contents of volcanic soils; Wright et al. [2002] found the relationship between dielectric constants and water contents of hydrate-bearing sediments. Thereafter, TDR was effectively used to measure hydrate pore saturations of the hydrated sediments [Ye et al., 2008; Hu et al., 2010].
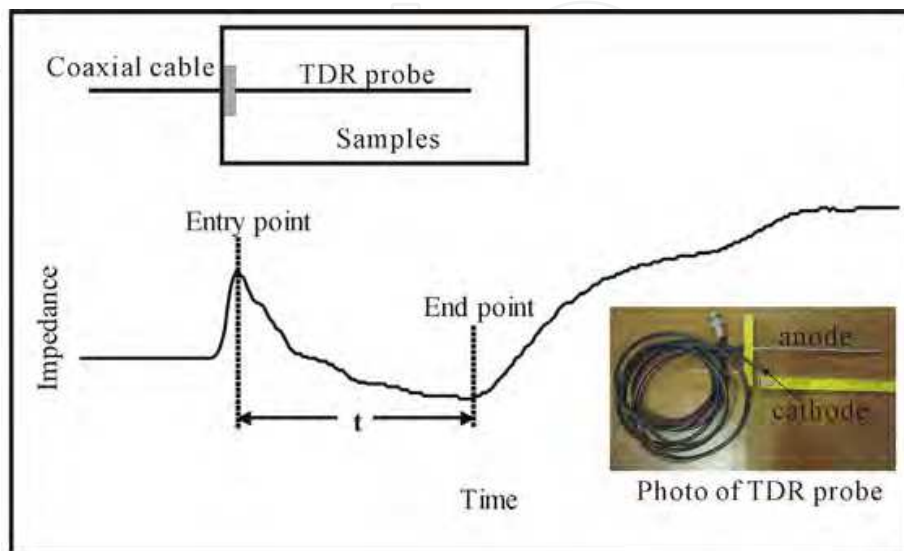

Fig. 3. TDR waveform of low-salty sediments with traditional TDR probe

TDR waveform of a soil or sediment sample is shown in Fig 3. The electromagnetic wave is generated by TDR instruments, and transmitted along the coaxial cable and the TDR probe (Fig 1 & Fig 3). Because there is loss current during electromagnetic wave transmitting in the samples, the characteristics of the entry point and the end point are obviously. The velocity of electromagnetic wave transmitting in the samples can be calculated with:

$$V = 1 / t \qquad (1)$$

Where l is the length of the TDR probe, t is the time-interval between entry point and end point (Fig 3). At the same time, the velocity of electromagnetic wave in the samples can be also related to dielectric constants:

$$V = c / Ka^{1/2} \qquad (2)$$

Where c is the velocity of propagation in free space (approximately 3×10^8 m/s). From equation 1 and 2 it solves:

$$Ka = [ct / l]^2 \qquad (3)$$

When the Ka is calculated, with the relationship between Ka and water contents we can obtain the water contents of the sample. For soils [Topp et al.,1980]:

$$\theta v = -5.3 \times 10^{-2} + 2.92 \times 10^{-2} Ka - 5.5 \times 10^{-4} Ka^2 + 4.3 \times 10^{-6} Ka^3 \qquad (4)$$

For hydrate-bearing sediments, it's effective to use Wright et al. [2002] 's empirical equation:

$$\theta v = -11.9677 + 4.506072566Ka - 0.14615Ka^2 + 0.0021399Ka^3 \tag{5}$$

As a result, the hydrate pore saturation of the hydrated sediments can be calculated with:

$$Sh=(\varphi-\theta v)/ \; \varphi \times 100\% \tag{6}$$

Where φ is the porosity of the sample.

2.1.3 Synthesized method of hydrated sediments

Gas hydrates could be formed in sediments by at least four different methods in many types of apparatus. Gas can be introduced to specimens containing (1) partially water-saturated sediment [Waite et al., 2004], (2) water-saturated sediment [Winters et al., 2007], (3) seed ice-sediment [Priest et al., 2005] and (4) continually feeding gas-saturated water into the specimen, which is rarely used because of much difficult and time-consuming. The "gas + water-saturated sediment" system was used to synthesize hydrate-bearing sediments in this study.

The geophysical experimental apparatus in the Gas Hydrate Laboratory of Qingdao Institute of Marine Geology (GHL-QIMG) [Ye et al., 2005, 2008; Hu et al., 2010] can simulate in situ pressure and temperature conditions conducive to hydrate formation (Fig. 4). The apparatus is composed of five functioning units: (1) A high-pressure vessel with a plastic inner barrel for simulating in situ pressure and temperature, in which there are two platinum (Pt100) resistance thermometers with precision of ±0.1°C used for measuring the temperature of inner and surface of the sample. (2) a vessel used for making gas-saturated water, (3) a gas compressor and a pressure transducer (precision, ±0.1MPa) responsible for gas pressure control, (4) a cooling system and a bathing through for temperature control , and (5) a computer system for measuring and logging data.
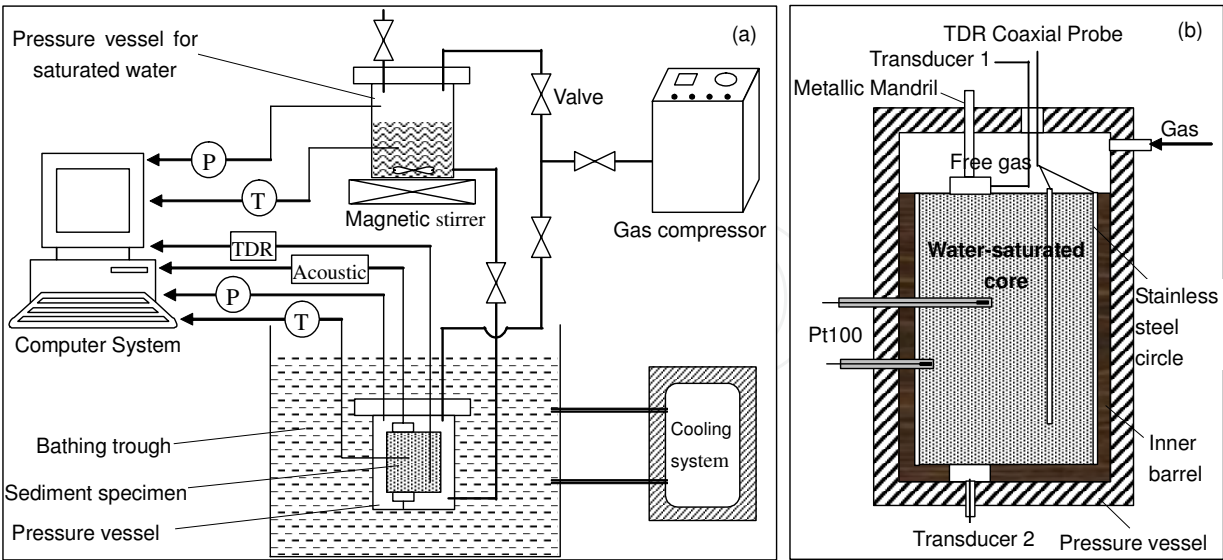

Fig. 4. Schematic diagram of experimental apparatus for geophysical research on gas hydrate-bearing sediments.

The experimental processes are as follows: (1) the artificial core was immersed by pure water or 300ppm SDS solution to gravimetric water content of about 40%, and then loaded

into the high-pressure vessel; (2) Methane gas was introduced into the vessel to a scheduled pressure after vacuum, and more than 24 hours are allowed for methane dissolving into the fluid; (3) Temperature in the high pressure-vessel was controlled to ~2°C for hydrate formation; and (4) Temperature was increased naturally to room temperature for hydrate dissociation.

During the whole process of hydrate formation and dissociation, real-time measurements on temperature, pressure, the ultrasonic waveform, and the TDR waveform were recorded by the computer system.

2.2 Acoustic properties of hydrate-bearing consolidated sediments

During gas hydrate formation and subsequent dissociation in the consolidated sediments, the acoustic properties of the sample were measured and the phenomenon is described below. Also, with the results we obtain the relationship between hydrate saturations and acoustic properties of the hydrate-bearing consolidated sediments.

2.2.1 Hydrate formation and dissociation processes

Methane gas was charged into the specimen until the pressure reached to ~5MPa. Then the temperature was decreased gradually and finally at 5°C hydrates began to form (Fig. 5). A temperature-anomaly could be detected in the sample due to the exothermic reaction when hydrate forms. At the same time, the decrease of water content and pressure also indicated that hydrates began to form. In order to get more hydrates, we kept the temperature-pressure condition of the high-pressure vessel for 1~2d. The hydrate saturations range from 0% to 65.5% (water content 40.18% to 13.85%). Gas hydrate dissociation was induced by increasing temperature and the hydrate-dissociation process typically lasts about 8~10 hours.
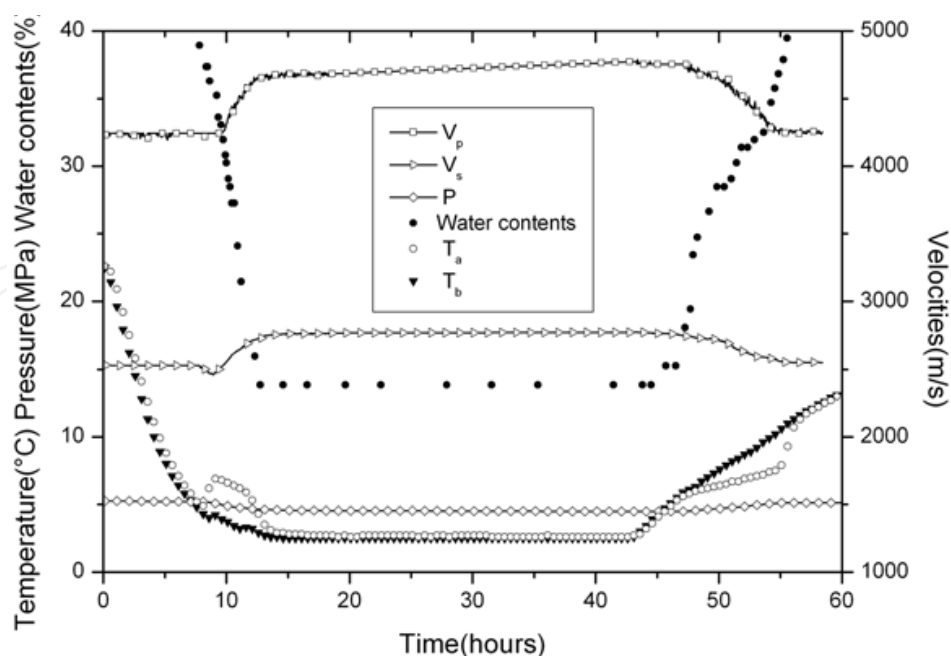

Fig. 5. Variation in temperature (T), pressure (P), water content and acoustic velocities (Vp&Vs) during gas hydrate formation and subsequent dissociation in the sediment core. Ta and Tb are temperatures of the inner and surface of the sediment core, respectively.

2.2.2 Acoustic properties

Figure 6 shows the changes of acoustic velocities (Vp, Vs) and hydrate saturations in hydrate-formation process. The Vp and Vs of the water-saturated sediment are 4242m/s and 2530m/s, respectively. During the first stage of hydrate-formation process, Vp changes hardly (time: 7.7h-~9.7h；Sh: 0-~20%). Later, it begins to increase and gets to 4643m/s when the hydrate saturation is up to ~65.5% (time: 12.75h). The Vs of the sediment decreases slightly to 2470m/s at the beginning of hydrate-formation process (time: 7.7h-8.95h; Sh: 0-~10%). After that it begins to increase and gets to 2725m/s when the hydrate saturation is up to ~65.5%. Although the pressure-temperature condition was maintained 1~2d after hydrate saturation up to 65.5%, the hydrate saturation didn't increase. However, both Vp and Vs increase slightly in hydrate-maintained process. Vp and Vs increase to 4770m/s and 2770m/s, respectively. During the hydrate-dissociation process, Vp and Vs of the sediments decrease with the increasing water contents (decreasing hydrate saturation). And they decrease to 4250m/s and 2550m/s respectively when gas hydrate was completely dissociated (Fig. 5).
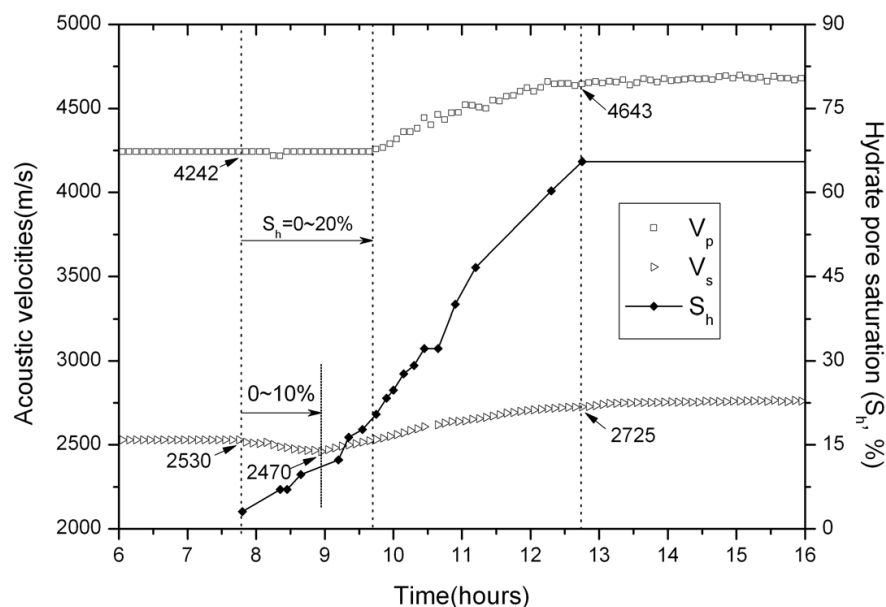

Fig. 6. Variation in hydrate saturation (Sh) and acoustic velocities (Vp & Vs) during gas hydrate formation. Vp changes very little during hydrate saturation 0~20%. Vs decrease from 2530m/s to 2470m/s during hydrate saturation 0~10%.

2.3 Relate hydrate saturation to acoustic velocities

The compressional (or shear) wave velocity measured in the hydrate-dissociation process is much higher than that measured in the hydrate-formation process at the same saturation degree. It may be caused by the hydrate morphology. As indicated in Yoslim and Englezos [2008], when surfactant (SDS) is present in the system, porous hydrate is believed to form at the gas-water interface. In addition, hydrate formation may occur in two stages: first the formation of a water-hydrate slurry, and then a very slow solidification stage [Beltrán and Servio, 2008]. Thus, in the hydrate formation process, the hydrates are porous and soft; as time lapses, the hydrates become rigid solids and consequently lead to an increase of the

velocity. Because it's difficult to judge whether in situ gas hydrates are in the process of formation or dissociation during gas hydrate exploration, we use the average Vp (or Vs) of the compressional (or shear) wave velocities obtained in the two processes as the measured velocity to relate with gas hydrate saturations in this paper (Fig. 7). The result shows that acoustic velocities are insensitive to low hydrate saturations (0-~10%). However, the velocities increase rapidly with hydrate saturation when saturation is higher than 10%, especially in the range of 10-30%.
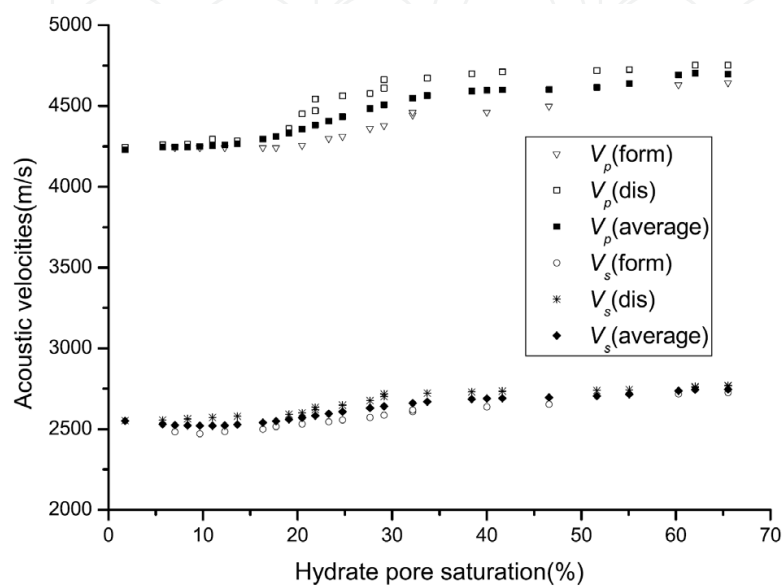
Fig. 7. Variation in Vp during hydrate formation (Vp(form)) and hydrate dissociation (Vp(dis)), Vs during hydrate formation (Vs(form)) and hydrate dissociation (Vs(dis)), the average Vp of Vp(form) and Vp(dis), and the average Vs of Vs(form) and Vs(dis).

3. Ultrasonic waves in hydrate-bearing unconsolidated sediments

The attenuation of ultrasonic wave in unconsolidated sediments is usually much higher than that in consolidated sediments. In order to obtain both Vp and Vs of the hydrate-bearing unconsolidated sediments, various techniques including bender elements, resonant column, etc, are developed to measure acoustic properties of the hydrated samples. In this section, the bender elements are successfully used in measuring both Vp and Vs of the hydrate-bearing unconsolidated sediments.
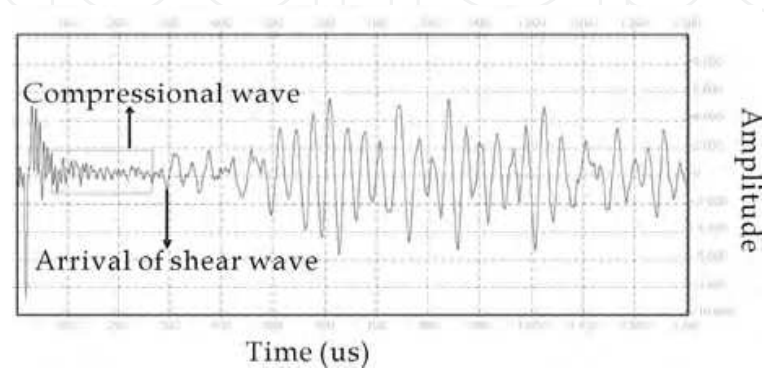

Fig. 8. Waveform of the hydrated unconsolidated sediments measured by bender elements

A waveform of the hydrated sediments measured by bender elements is shown in Fig. 8. From the waveform, it's easy to read the arrival time of shear wave. However, the arrival time of compressional wave is hard to get because of the noise. Thus, we combine the FFT transformation and wavelet-transformation (we called FFT-WT method hereafter) to interpret the compressional wave and obtain the Vp data. Calibration has been made and the method is considered to be correct.

3.1 Bender elements technique

Bender elements are commonly used to measure shear wave velocity of unconsolidated sediments. In order to obtain both Vp and Vs of the hydrate-bearing unconsolidated sediments, a new kind of bender element transducers are developed. With the FFT-WT method, the new transducers are used successfully in this study.

3.1.1 Preparation of bender element transducers

Bender elements consist of two sheets of piezoceramic plates rigidly bonded to a center shim of brass or stainless steel plate (Fig. 9a). When the "cantilever beam" of the transducer is excited by an input voltage, it changes its shape and generates a mechanical excitation (Fig. 9b), and then the signal transmits to the receiver bender element. The in-plane directivity of bender elements was explored by Lee and Santamarina (2005). The results show that amplitude of the signal is more pronounced when the installations of bender elements are parallel (Fig. 10). The amplitude in the transverse configuration is about 75% of the amplitude at 0° in the parallel axes configuration, which suggest the potential use of bender elements in a wide range of in-plane configurations besides the standard tip-to-tip alignment. In order to obtain good signal, we use the parallel installations in our experiments.
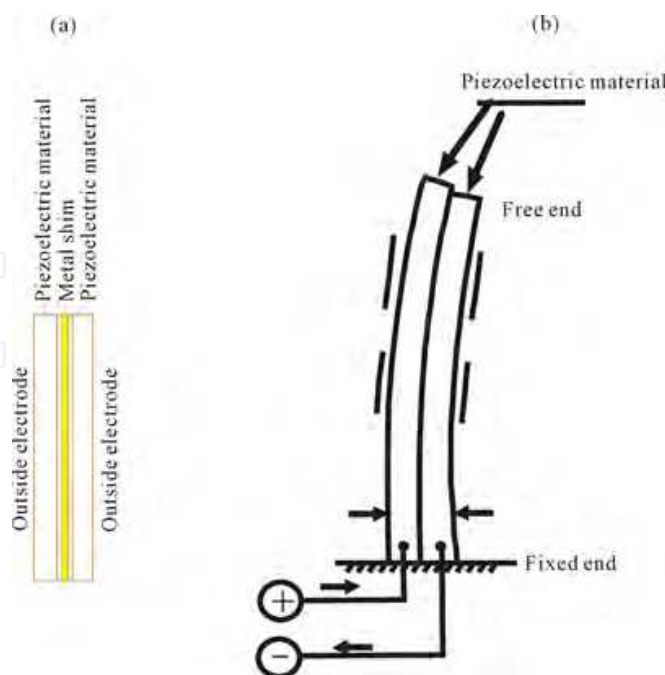

Fig. 9. (a) Schematic representation of bender element; (b) Mechanical excitation of bender element.
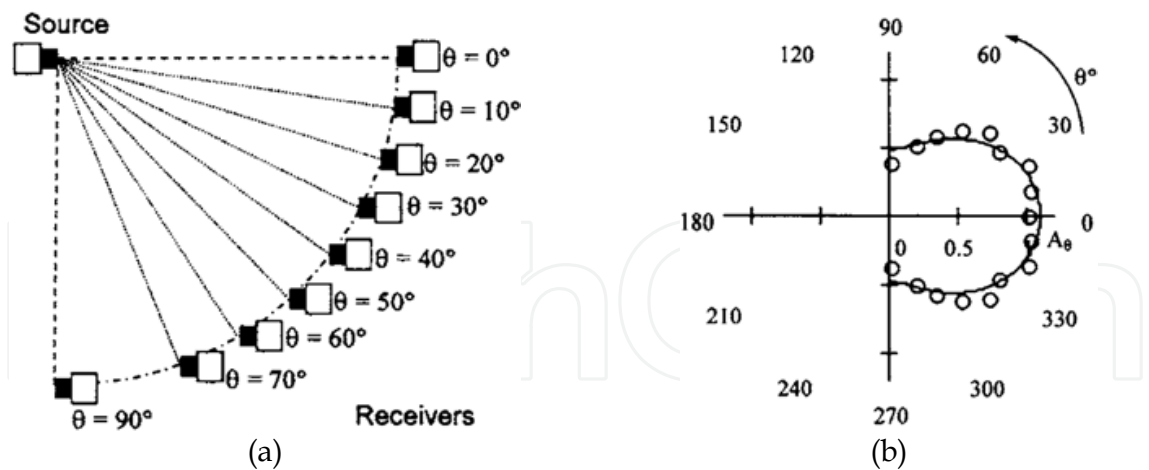
Fig. 10. Source-receiver directivity: (a) test setup, and (b) polar plot of peak amplitudes [Lee and Santamarina, 2005]
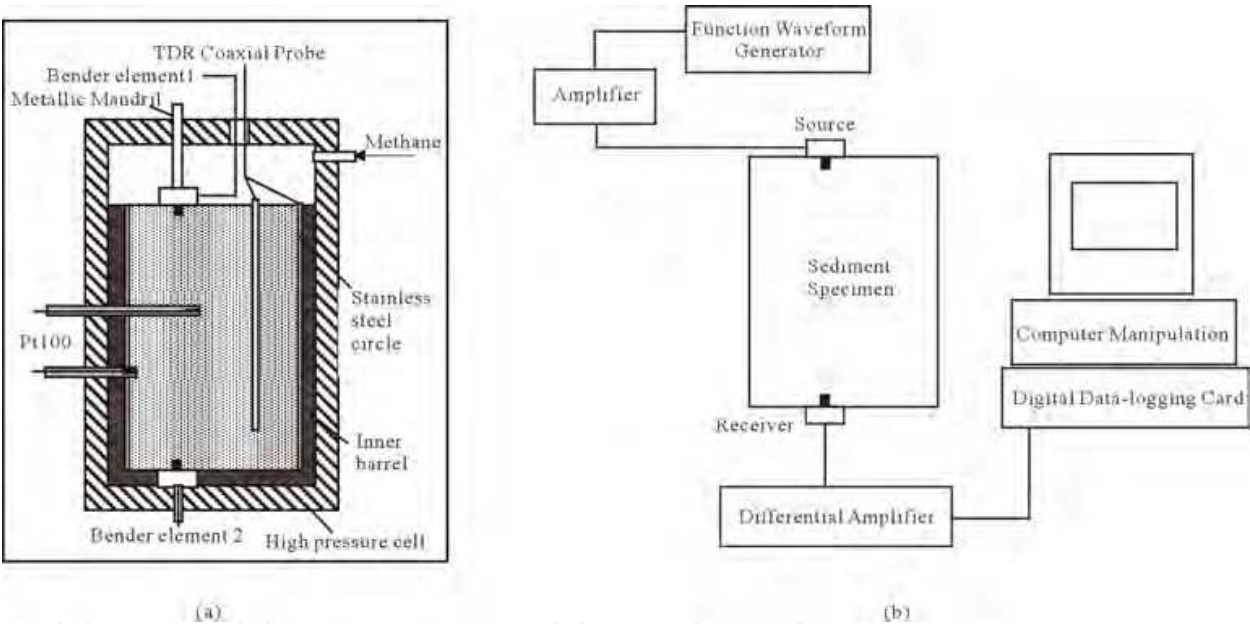

Fig. 11. (a) Schematic map of the high pressure cell for hydrate formation and acoustic measurements; (b) Measuring system of bender elements

Simultaneous measurements of compressional and shear wave velocity of methane hydrate bearing sediments using bender elements are explored. The apparatus is shown in Fig. 11. In the acoustic measuring system (Fig. 11b), signal is generated, amplified and then transmitted by the source bender element. Because the mechanical excitation of bender element is transverse, the waveform received by the receiver bender element is mainly shear wave. In order to obtain both shear wave and compressional wave, a new kind of bender element is developed (Fig. 12).

To overcome a high pressure environment, the bender elements are filled with phenolic resin and protected by stainless steel shell. The mechanical excitation of the new bender element is shown in Fig 12b. The cantilever beam is driven by two piezoelectric circles. When the excitation is generated, the cantilever beam will be distorted and the torsional

vibration is occurred. At the same time, a small longitudinal movement is also occurred on the cantilever beam. In order to magnify the longitudinal movement, we add a longitudinal piezoelectric slice clinging to the bender elements. Therefore, there is also compressional wave in the integrative waveform (Fig. 8). From the waveform, it's easy to read the first arrival of shear wave. However, as the noise is largely, we develop the FFT-WT method to analysis the first arrival time of compressional wave.
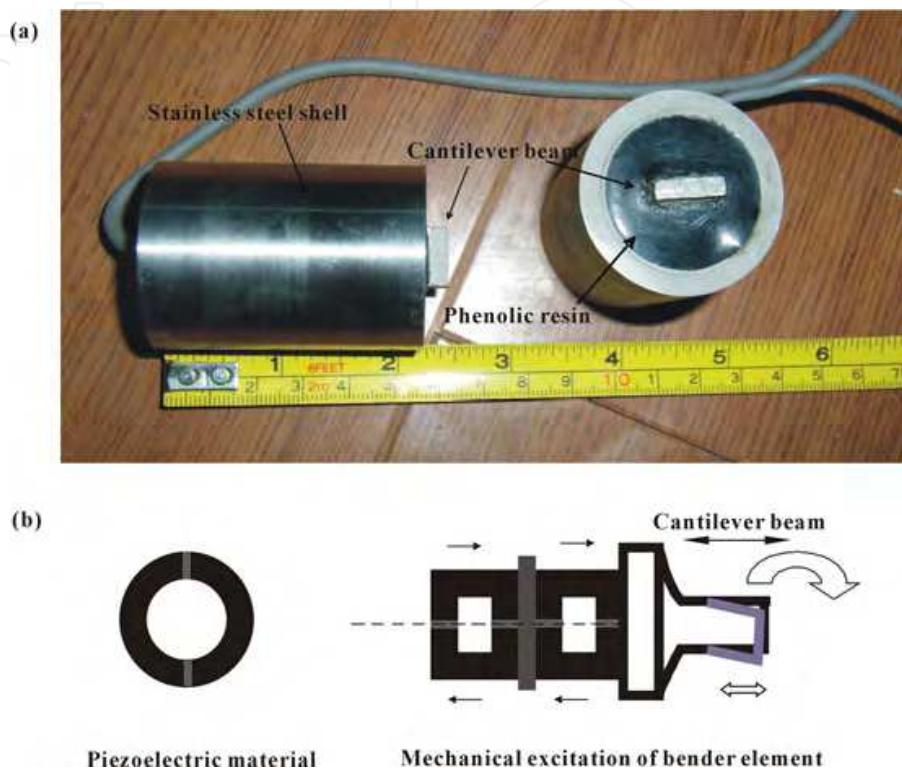
Fig. 12. (a) Photography of the bender element transducers; (b) mechanical excitation of the new bender element.

3.1.2 Calibration

Compressional and shear wave velocities are calculated with: $Vp=L_{tt}/(t_p-t_{0p})$, $Vs=L_{tt}/(t_s-t_{0s})$, where L_{tt} is the tip-to-tip distance of two bender elements, t_p and t_s are travel times of compressional wave and shear wave in the sediments respectively, t_{0p} and t_{0s} are the measured travel times of compressional wave and shear wave in the bender element transducers respectively. Four different lengths of cylindrical Polyoxy-methylene (POM) columns were used to calibrate t_{0p} and t_{0s} of the bender elements (Table 1). The diameter of the POM columns are about 6cm, which is close to the diameter of samples (6.8cm). The waveform of the POM column is shown in Fig. 13. It shows that it's easy to read both arrival times of the P-wave and S-wave using the new type of bender elements. According to lengths and wave-arrival times of the four POM columns, we obtained the t_{0p} and t_{0s}, which are 7.017us and 18.63us respectively. And the P-wave and S-wave velocities of the POM material are 2294.5m/s and 933.9m/s respectively [Fig. 14], which is very close to the reported values [Choy et al., 1983]. The P-wave velocity is also close to the measured results by our flat-plate transducers, which is 2280m/s for POM-I and 2319m/s for POM-II.

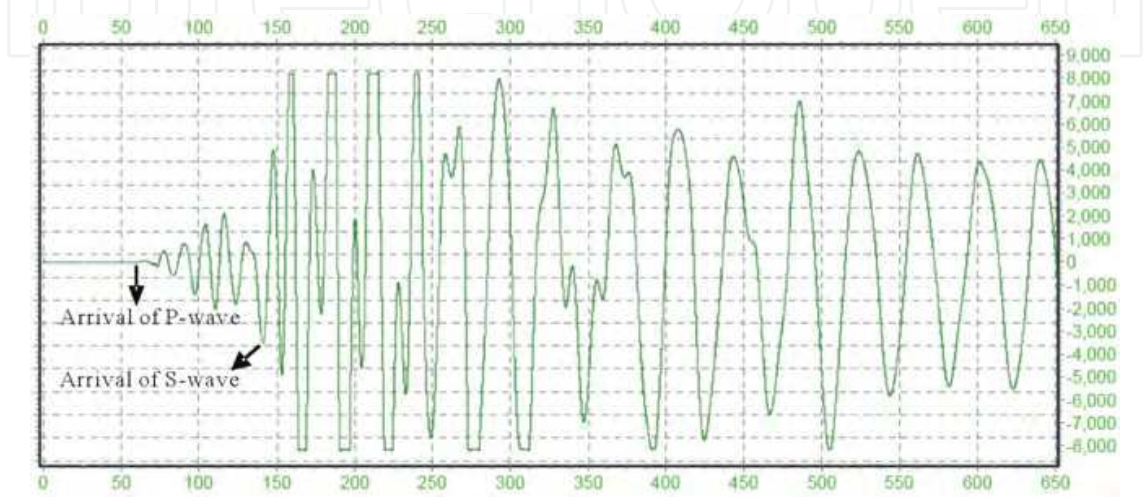| Number	Diameter (mm)	Length (mm)	Trough depth (mm)
POM-I	60.3	120	3.9~4.0
POM-II	60.3	150	3.9~4.0
POM-III	60.4	204	3.94
POM-IV	60.4	250	3.84

Table 1. Parameters of the POM columns
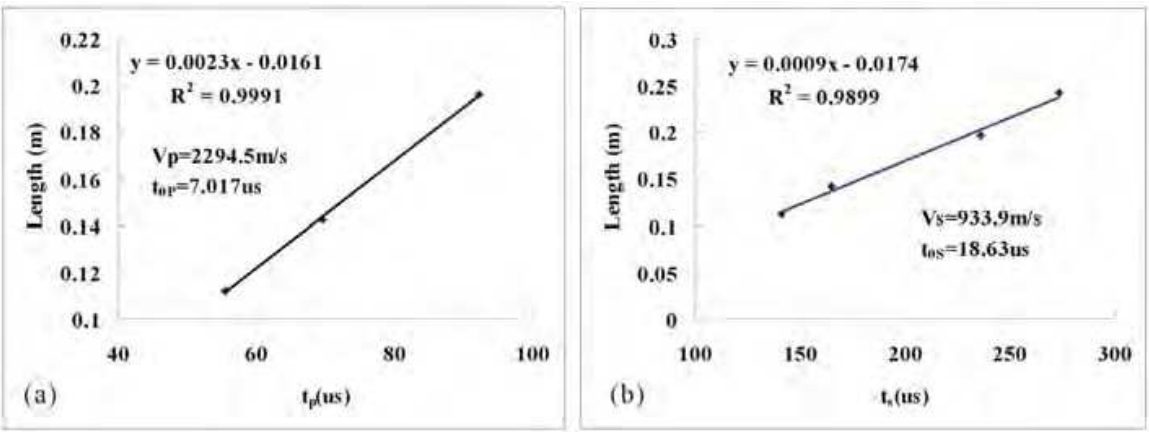

Fig. 13. Waveform of POM-I by bender element transducers

Fig. 14. Calibrating results of the new bender elements

3.1.3 FFT-WT method

Usually, there are two approaches to obtain the travel time of shear wave when using bender elements. In the first approach, the travel time can be directly read from the waveform of the receiver bender element. The characteristic point of wave's arrival must be very markedly when using this approach. The second approach is based on detailed analysis of the waveform, such as the Dynamic Finite Element Analysis, Cross-Correction Analysis, Phase Velocity Analysis, Phase Sensitive Detection, etc. Because it's easy to read the characteristic point of shear wave's arrival in our experiments, we used the first

approach to determine the travel time of shear wave. However, as compressional wave is significantly influenced by the acoustic noise of the samples, the FFT-WT method is developed to determine the travel time of compressional wave.

The analysis process is as follows: (1) measuring the main frequencies of the bender element transducers; (2) choosing the compressional waveform, make a Fast Fourier Transform (FFT) on the waveform to obtain the main frequency of compressional wave; (3) making Wavelet Transform (WT) on the chosen compressional waveform to obtain frequencies versus arrival time, from which the arrival time of compressional wave can be obtained. An example of the analysis process is given below.

Firstly, the frequencies of the bender element transducers are determined by admittance curves. The results indicate that the main shear frequency is 30kHz, while the main compressional frequencies are 75kHz, 125kHz, and 140kHz. Secondly, the frequency of compressional wave is analyzed by FFT (Fig. 15). It shows that the frequencies of compressional wave mainly consist of 122kHz and 73kHz. Thirdly, the chosen compressional waveform is analyzed by WT (Fig. 16). With the frequency versus arrival time by WT, it shows that at about 96.1µs the frequency characteristics are the same with that analyzed by FFT. Thus, the travel time of compressional wave is 96.1µs with the above FFT-WT analysis.

Using above FFT-WT method, the travel time of shear wave can be also obtained. The results of Vs obtained using FFT-WT method are comparable with that measured by the first approach (in which the travel time of shear wave is read directly) (Fig. 17), which indicates that the FFT-WT method is credible.
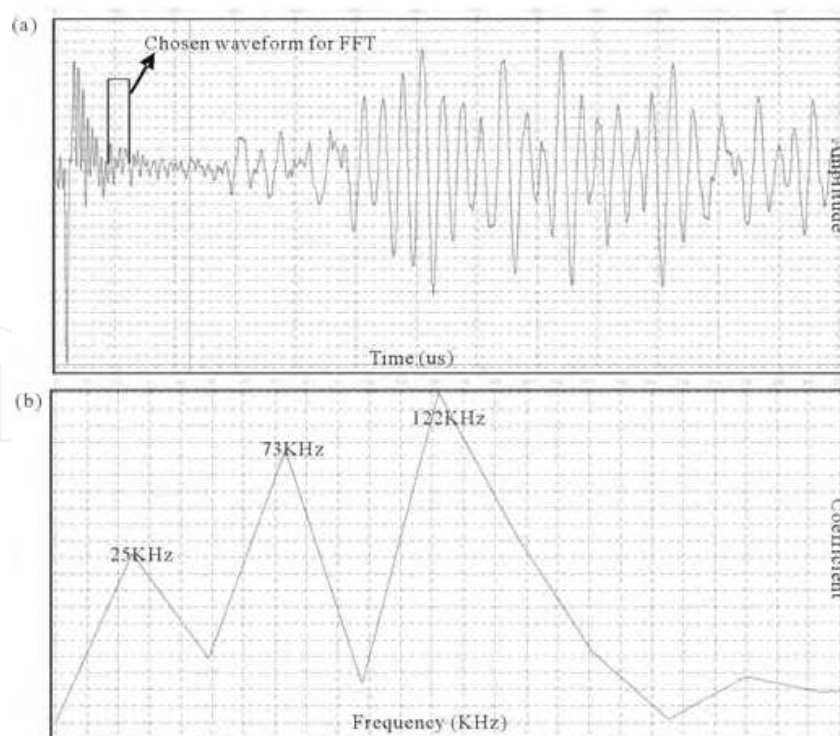

Fig. 15. (a) chosen compressional waveform for FFT analysis; (b) main frequencies of compressional wave
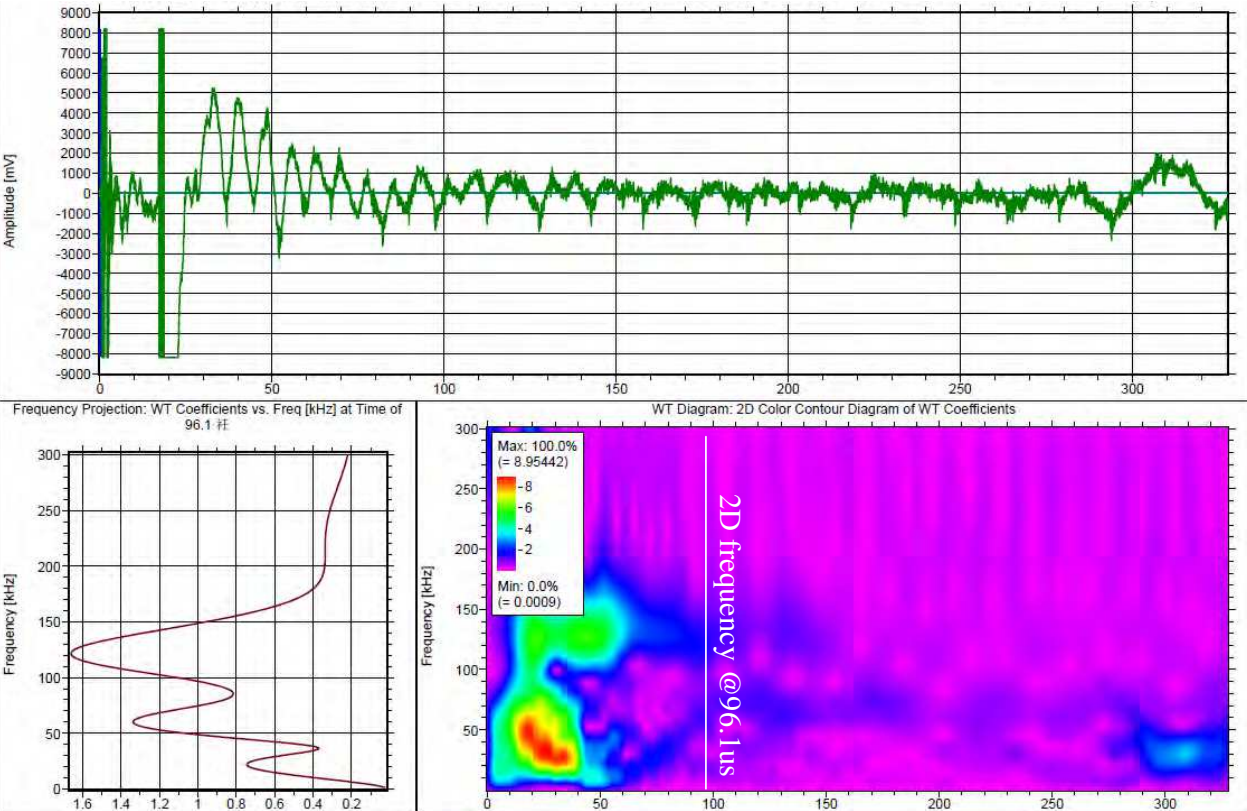
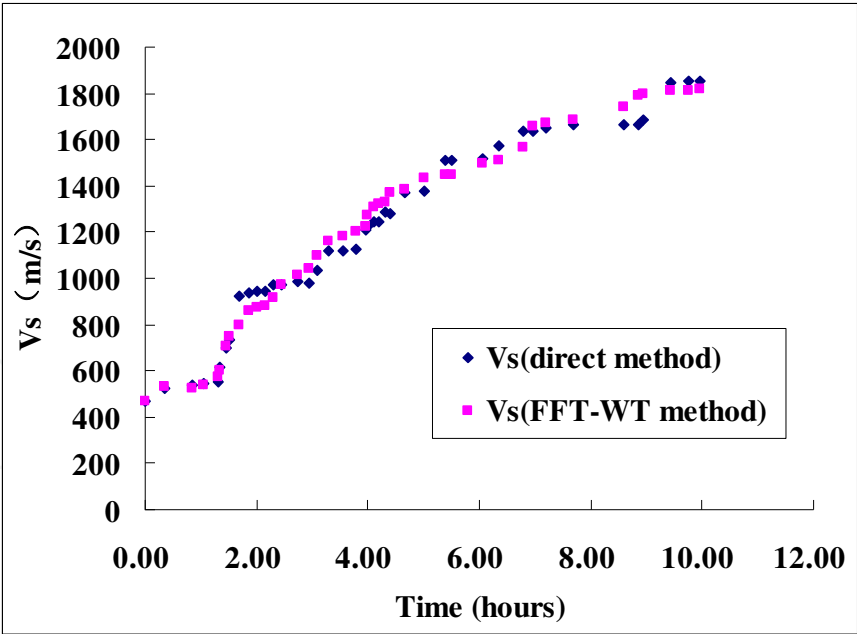Fig. 16. WT analysis of waveform by bender element measurement

Fig. 17. Comparison of Vs determined by the direct method and the FFT-WT method

3.2 Acoustic properties of hydrate-bearing unconsolidated sediments

Methane hydrate was formed and then dissociated in the 0.09~0.125mm sands (with saturated water), during the process the acoustic velocities (Vp and Vs) of the samples are

measured simultaneously with the new type of bender element transducers and analyzed with the FFT-WT method. Also, the water content, temperature, pressure of the porous media are measured (Fig. 18). The results show that the time point of gas hydrates begin to form (or dissociate) detected by the acoustic velocities is the same with that detected by the temperature-pressure method, which indicates that the bender element technique is very sensitive with gas hydrate formation and dissociation. Thus, it is effective for using the new type of bender elements in measuring both Vp and Vs of hydrate-bearing unconsolidated sediments under high pressure conditions.
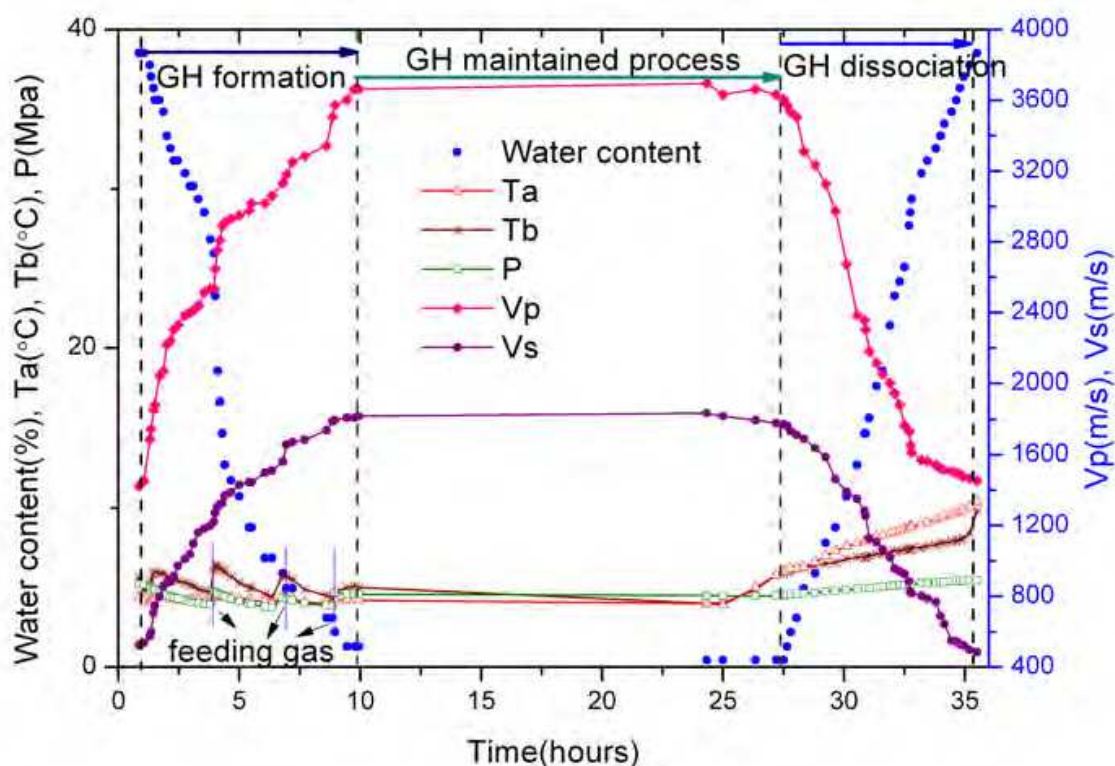

Fig. 18. Changes of parameters during gas hydrate formation and subsequent dissociation

The experimental results also show that the compressional (or shear) wave velocity measured in the hydrate-dissociation process is much lower than that measured in the hydrate-formation process at the same saturation degree (Fig. 19). This may be caused by the influence of gas hydrates on the sediment frame. In the unconsolidated sediments, gas hydrates may act as a kind of cement. A small amount of gas hydrates may dramatically affects the acoustic velocities in this condition (Priest et al., 2005). During gas hydrate formation and dissociation in the unconsolidated sediments, the influences of gas hydrates on the sediment frame became smaller as time lapse. As a result, compressional (or shear) wave velocity of the hydrated unconsolidated sediments in the hydrate-dissociation process is lower than that in the hydrate-formation process. With the average Vp (or Vs) of the compressional (or shear) wave velocities obtained in the two processes, we obtained the relationship between gas hydrate saturation and acoustic velocities of hydrate-bearing unconsolidated sediments. The result shows that Vp and Vs increase rapidly with hydrate saturations, although they increase relatively slow in the range of saturation 25%~60%. It indicates that gas hydrate may first cement grain particles of the unconsolidated sediments,

when hydrate saturation is higher, gas hydrate may contact with the sediment frame, or continue cementing sediment particles.
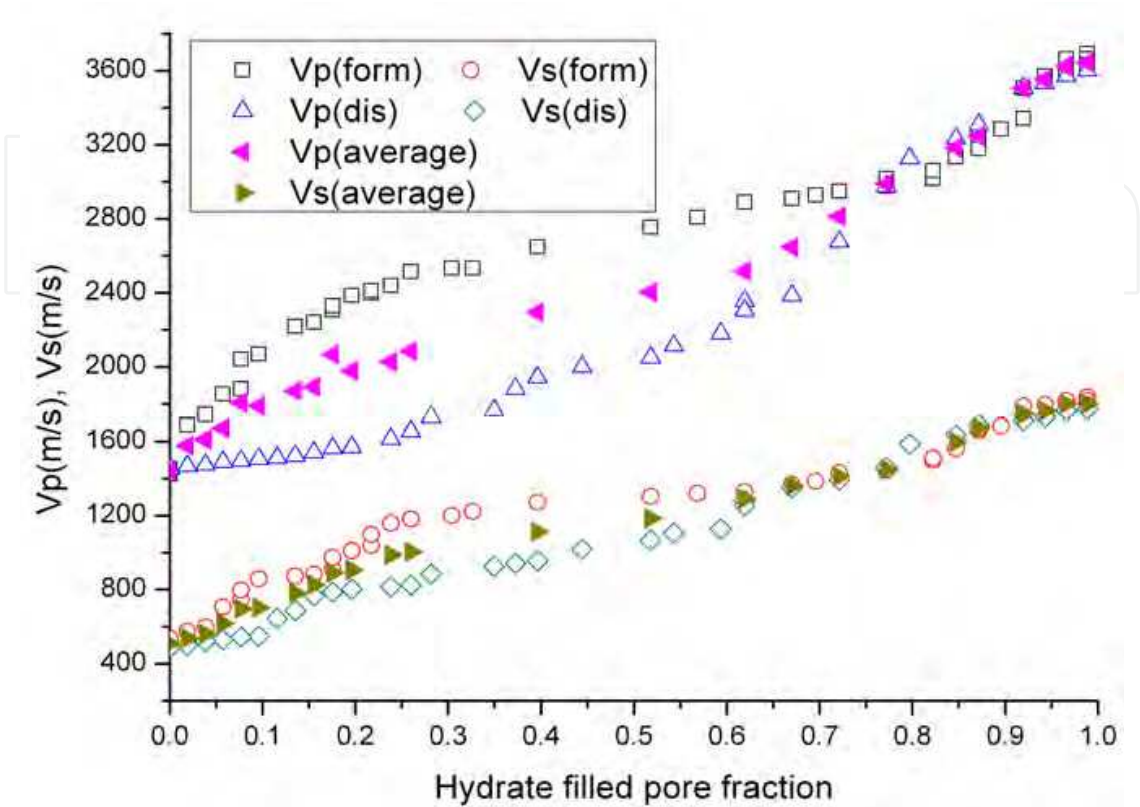

Fig. 19. For unconsolidated sediments: variation in Vp during hydrate formation (Vp(form)) and hydrate dissociation (Vp(dis)), Vs during hydrate formation (Vs(form)) and hydrate dissociation (Vs(dis)), the average Vp of Vp(form) and Vp(dis), and the average Vs of Vs(form) and Vs(dis).

4. Discussions and conclusions

Some interesting acoustic phenomena have been observed in the above experiments. For example, we noticed that compressional (or shear) wave velocities are different at the same saturation degree during hydrate-formation process and hydrate-dissociation process. The morphology of gas hydrates may be a possible factor. As discussed above, hydrate formation may occur in two stages: first the formation of a water-hydrate slurry and then a very slow solidification stage. In the consolidated sediments, gas hydrates became more and more rigid as time lapse during hydrate formation and dissociation. Thus, although the amounts of gas hydrates is the same, compressional (or shear) wave velocity in the hydrate-dissociation process is much higher than that in the hydrate-formation process. However, in the unconsolidated sediments, gas hydrates may act as a kind of cement which mainly affects the sediment frame. A small amount of gas hydrates may dramatically affects the acoustic velocities in this condition (Priest et al., 2005). During gas hydrate formation and dissociation in the unconsolidated sediments, the influences of gas hydrates on the sediment frame became smaller as time lapse. As a result, compressional (or shear) wave velocity of the hydrated unconsolidated sediments in the hydrate-dissociation process is lower than

that in the hydrate-formation process. The experimental results may provide basic knowledge for field geophysical interpretations.

In this chapter, two kinds of ultrasonic methods, namely, the flat-plate transducers and a new kind of bender elements have been successfully used in measuring the acoustic properties of gas hydrate bearing sediments. The results show that it's an effective way to use classic flat-plate transducers to measure both Vp and Vs of the consolidated sediments. However, in unconsolidated sediments the bender element technique is much appropriate because the bender elements can sustain larger attenuation. Thus, although significant attenuation was occurred during the unconsolidated experimental process, a developed FFT-WT method is capable of reading the time of the first arrival of P-wave, while the S-wave can be read directly.

Both methods have shown sensitivity in detecting the formation and dissociation of gas hydrate in sediments. With the flat-plate transducers, the acoustic properties of the hydrate bearing consolidated sediments were obtained, which shows that acoustic velocities are insensitive to low hydrate saturations but they increase rapidly with hydrate saturation when saturation is higher than 10%, especially in the range of 10-30%. The measurements by bender element technique figure out that Vp and Vs of the unconsolidated sediments increase rapidly with hydrate saturations, although they increase relatively slow in the range of saturation 25%~60%. It indicates that gas hydrate may first cement grain particles of the unconsolidated sediments, and then contact with the sediment frame.

5. Acknowledgment

6. References

Sloan, E. D., Jr. (1998), *Clathrate Hydrates of Natural Gases*, CRC Press, Boca Raton, Fla.

Kvenvolden, K. A. (1998), *A primer on the geological occurrence of gas hydrate*, Geological Society, London, Special publications, 137, 9-30.

Milkov, A. V., and R. Sassen (2003), Preliminary assessment of resources and economic potential of individual gas hydrate accumulations in the Gulf of Mexico continental slope, *Marine and Petroleum Geology*, 20, 111–128.

Dickens, G. R. (2003), A methane trigger for rapid warming?, *Science*, 299, 1017.

Dickens, G. R. (2004), Hydrocarbon-driven warming, *Nature*, 429, 513-515.

Brown, H. E., W. S. Holbrook, M. J. Hornbach and J. Nealon (2006), Slide structure and role of gas hydrate at the northern boundary of the Storegga Slide, offshore Norway, *Marine Geology*, 229, 179-186.

Pecher, I., R. F. Ayoub, and B. Clennell (2008), Seismic time-lapse monitoring of potential gas hydrate dissociation around boreholes – could it be feasible? A conceptual 2D study linking geomechanical and seismic FD models, *paper presented at Sixth International Conference on Gas Hydrate*, Brithish Columbia, Canada.

Shipley, T. H., M. H. Houston, R. T. Buffler, F. J. Shaub, K. J. McMillen, J. W. Ladd, and J. L. Worzel (1979), Seismic evidence for widespread occurrence of possible gas hydrate horizons on continental slopes and rises, *AAPG Bull.*, 63(12), 2204-2213.

Holbrook, W. S., H. Hoskins, W. T. Wood, R. A. Stephen, and D. Lizarralde (1996), Methane hydrate and free gas on the Blake Ridge from Vertical Seismic Profiling, *Science*, 273, 1840-1843.

Carcione, J. M., and D. Gei (2004), Gas-hydrate concentration estimated from P- and S-wave velocities at the Mallik 2L-38 research well, Mackenzie Delta, Canada, *Journal of Applied Geophysics*, 56, 73-78.

Stoll, R. D.(1974), Effects of gas hydrate in sediments, in *Natural Gases in Marine Sediment*, edited by I. Kaplan, pp. 235-248, Springer, New York.

Tucholke, B. E., G. M. Bryan, and J. I. Ewing (1977), Gas hydrate horizons detected in seismic-profile data from the western North Atlantic, *Am. Assoc. Petrol. Geol. Bull.*, 61, 698-707.

Wyllie, M. R. J., A. R. Gregory, and G. H. F. Gardner (1958), An experimental investigation of factors affecting elastic wave velocities in porous media, *Geophysics*, 23, 459-493.

Pearson, C. F., P. M. Halleck, P. L. McGulre, R. Hermes, and M. Mathews (1983), Natural gas hydrate; A review of in situ properties, *J. Phys. Chem.*, 87, 4180-4185.

Wood, A. B. (1941), *A text book of sound*, Macmillan, New York, 578 pp

Lee, M. W., D. R. Hutchinson, T. S. Collett and W. P. Dillon (1996), Seismic velocities for hydrate-bearing sediments using weighted equation, *J. Geophys. Res.*, 101, 20347-20358.

Helgerud, M. B., J. Dvorkin, A. Nur, A. Sakai, and T. Collett (1999), Elastic-wave velocity in marine sediments with gas hydrate: Effective medium modeling, *Geophysical Research Letters*, 26, 2021-2024.

Dvorkin, J., and M. Prasad (1999), Elasticity of marine sediments: Rock physics modeling, *Geophysical research letters*, 26(2), 1781-1784.

Lee, M. W. (2002a), Biot-Gassmann theory for velocities of gas hydrate-bearing sediments. *Geophysics*, 67, 1711-1719.

Lee, M. W. (2002b), Modified Biot-Gassmann theory for calculating elastic velocities for unconsolidated and consolidated sediments, *Marine Geophysical Researches*, 23, 403-412.

Lee, M. W. (2003), *Velocity ratio and its application to predicting velocities*, U. S. Geological Survey Bulletin 2197, 19 pp., U. S. Geological Survey.

Chand, S., T. A. Minshull, D. Gei, and J. M. Carcione (2004), Elastic velocity models for gas-hydrate-bearing sediments-a comparison, *Geophys. J. Int.*, 159, 573-590.

Carcione, J. M., and U. Tinivella (2000), Bottom-simulating reflectors: seismic velocities and AVO effects, *Geophysics*, 65(1), 54-67.

Gei, D., and J. M. Carcione (2003), Acoustic properties of sediments saturated with gas hydrate, free gas and water, *Geophys. Prospect.*, 51, 141-157.

Jakobsen, M., J. A. Hudson, T. A. Minshull, and S. C. Singh (2000), Elastic properties of hydrate-bearing sediments using effective medium theory, *J. Geophys. Res.*, 105, 561-577.

Ojha, M., and K. Sain (2008), Appraisal of gas-hydrate/free-gas from Vp/Vs ratio in the Makran accretionary prim, *Marine and Petroleum Geology*, 25, 637-644.

Sothcott, J., C. McCann, and S. G. O'Hara (2000), The influence of two different pore fluids on acoustic properties of reservoir sandstones at sonic and ultrasonic frequencies, *paper presented at 70th Ann. Mtg., SEG*, Calgary, Exp. Abst., 2, 1883-1886.

Topp G C, Davis J L, Annan A P (1986). Electromagnetic determination of soil-water content：Measurement in coaxial transmission line. *Water Resour. Res.*, 1980, 16(3)：574-582.

Dalton F N, van Genuchten M T. The time domain reflectometry for measuring soil water content and salinity. *Geoderma*, 38: 237-250.

Ye Y G, Zhang J, Hu G W, et al (2008). Combined detection technique of ultrasonic and time domain reflectometry in gas hydrate. *Marine Geology & Quaternary Geology (in Chinese with English abstracts)*, 28(5): 101-107.

Hu G W, Ye Y G, Zhang J, et al (2010). Acoustic properties of gas hydrate-bearing consolidated sediments and experimental testing of elastic velocity models. *Journal of Geophysical Research*, 115: B02102. doi: 10.1029/2008JB006160.

Ye Y G, Zhang J, Hu G W, et al (2008). Experimental research on the relationship between gas hydrate saturation and acoustic parameters. *Chinese Journal of Geophysics*, 51(4): 819-828.

Regalado C M (2003). Time domain reflectometry models as a tool to understand the dielectric response of volcanic soils. Geoderma, 117:313-330.

Wright J F, Nixon F M, Dallimore S R, et al (2002). A method for direct measurement of gas hydrate amounts based on the bulk dielectric properties of laboratory test media. *Fourth International Conference on Gas Hydrate*, Yokohama, 745-749.

Waite, W. F., W. J. Winters, and D. H. Mason (2004), Methane hydrate formation in partially water-saturated Ottawa sand, *American Mineralogist*, 89, 1202-1207.

Winters, W. J., W. F. Waite, D. H. Mason, L. Y. Gilbert, and I. A. Pecher (2007), Methane gas hydrate effect on sediment acoustic and strength properties, *Journal of Petroleum Science and Engineering*, 56, 127-135.

Ye, Y. G., C. L. Liu, S. Q. Liu, J. Zhang, and S. B. Diao (2005), Experimental studies on several significant problems related marine gas hydrate, *paper presented at Fifth International Conference on Gas Hydrate*, Trondheim, Norway.

Yoslim, J., and P. Englezos (2008), The effect of surfactant on the morphology of methane/propane clathrate hydrate crystals, *paper presented at Sixth International Conference on Gas Hydrate*, Brithish Columbia, Canada.

Beltrán, J. G., and P. Servio (2008), Morphology studies on gas hydrates interacting with silica gel, *paper presented at Sixth International Conference on Gas Hydrate*, Brithish Columbia, Canada.

Lee J S, Santamarina J C (2005). Bender elements: Performance and signal interpretation. *Journal of Geotechnical and Geoenvironmental Engineering*, 1063-1070.

Choy C L, Leung W P, and Huang C W (1983). Elastic moduli of highly oriented polyoxymethylene. *Polymer Engineering and Science*, 23(16): 910-922.

Priest, J., C. R. I. Best, and R. I. Clayton (2005), A laboratory investigation into the seismic velocities of methane gas hydrate-bearing sand, *J. Geophys. Res.*, 110, B04102, doi:10.1029/2004JB003259.
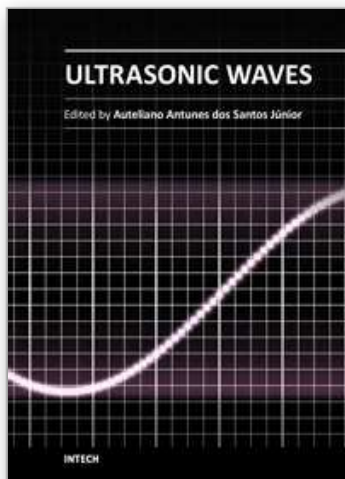
Ultrasonic Waves

Edited by Dr Santos

Ultrasonic waves are well-known for their broad range of applications. They can be employed in various fields of knowledge such as medicine, engineering, physics, biology, materials etc. A characteristic presented in all applications is the simplicity of the instrumentation involved, even knowing that the methods are mostly very complex, sometimes requiring analytical and numerical developments. This book presents a number of state-of-the-art applications of ultrasonic waves, developed by the main researchers in their scientific fields from all around the world. Phased array modelling, ultrasonic thrusters, positioning systems, tomography, projection, gas hydrate bearing sediments and Doppler Velocimetry are some of the topics discussed, which, together with materials characterization, mining, corrosion, and gas removal by ultrasonic techniques, form an exciting set of updated knowledge. Theoretical advances on ultrasonic waves analysis are presented in every chapter, especially in those about modelling the generation and propagation of waves, and the influence of Goldberg's number on approximation for finite amplitude acoustic waves. Readers will find this book ta valuable source of information where authors describe their works in a clear way, basing them on relevant bibliographic references and actual challenges of their field of study.

How to reference

In order to correctly reference this scholarly work, feel free to copy and paste the following:

INTECH
open science | open minds